Presented at the 36th European PV Solar Energy Conference and Exhibition, 9-13 September 2019, Marseille, France

IMPACT OF $POCL_3$ DIFFUSION PROCESS PARAMETERS ON OXYGEN PRECIPITATION IN CZOCHRALSKI-GROWN SILICON

S. Maus[1], S. Lohmüller[1], D. Mu[1], J. Schön[1;2], T. Niewelt[1;2], A. Wolf[1], R. Preu[1]
[1]Fraunhofer Institute for Solar Energy Systems ISE, Heidenhofstraße 2, 79110 Freiburg, Germany
[2]Laboratory for Photovoltaic Energy Conversion, Department of Sustainable Systems Engineering (INATECH), University of Freiburg, Emmy-Noether-Straße 2, 79110 Freiburg, Germany
Phone: +49 (0)761 4588 2186; e-mail: stephan.maus@ise.fraunhofer.de

ABSTRACT: Oxygen precipitates can be formed in Czochralski-grown silicon (Cz-Si) wafers during high temperature processes. They decrease the bulk charge carrier lifetime and thereby reduce the efficiency of the affected devices. The most relevant process for passivated emitter and rear cells is the $POCl_3$ diffusion. Therefore the influence of its process parameters on oxygen precipitation is highly relevant for industrial cell manufacturing. In this work, we investigate the impact of distinct $POCl_3$ diffusion parameters on oxygen precipitation in both p-type and n-type Cz-Si. A full factorial variation of the drive-in parameters, such as temperature and duration, based on an industry relevant $POCl_3$ diffusion process, is performed. The results show that the recombination activity of oxygen precipitates is increasing with both the temperature and the duration of the drive-in sequence. The oxygen diffusion length L_{Oi} during the process is identified to be a well-suited measure for the growth of oxygen precipitates in susceptible material and a threshold of $L_{Oi} < 0{,}3$ µm is proposed to limit detrimental effects on device performance. Similar trends for the oxygen precipitation were observed for p-type and n-type doped Cz-Si.
Keywords: Oxygen precipitate, $POCl_3$ diffusion, Defects, Czochralski, PERC

1 INTRODUCTION

Due to the higher potential in cell efficiency in comparison to the conventional aluminum back-surface field solar cells (Al-BSF), passivated emitter and rear cells (PERC) have gained more and more relevance for both, research institutes and industry [1]. However, PERC cells exhibit a high sensitivity towards changes in the bulk charge carrier lifetime τ_B [2], denoted as bulk lifetime in the following. Oxygen precipitates in crystalline silicon are known to enhance recombination [3] and thereby reduce τ_B along with boron oxygen defects [4] and other impurities [5]. Typically, precipitate nuclei in the form of aggregates of a few O atoms exist in as-cut state of silicon wafers [6, 7]. About 4% of current commercial Czochralski-grown silicon (Cz-Si) wafers [8], both p-type and n-type, include precipitate nuclei, which then form oxygen precipitates due to high temperature processes such as the $POCl_3$ diffusion. Oxygen precipitates lead to the formation of circular defect patterns in Cz-Si [8, 9], which reduce the cell efficiency of different p-type solar cell types, for instance PERC cells, as well as n-PERT cells up to 5% [3] and 1.5% absolute [10], respectively.

To reach a more sustainable production of PERC cells, a $POCl_3$ diffusion process not only needs to fulfill the requirements for an emitter with low recombination and low specific contact resistance, but also needs to prevent oxygen precipitation. Therefore, the influence of $POCl_3$ diffusion process parameters on oxygen precipitation in Cz-Si is highly relevant for industrial cell manufacturing. In this work, a full factorial variation of the drive-in parameters, such as temperature and duration, based on an industry relevant $POCl_3$ diffusion process, is performed and the effect on oxygen precipitation and consequently on τ_B is analyzed for different Cz-Si materials.

2 THEORY

The concentration of electrically active thermal donors (TDs) is an indirect measure of vacancy rich material`s susceptibility to form oxygen precipitates [10]. This is based on the strong indicative power of thermal donor concentration on both the overall oxygen concentration level and the thermal history during crystal growth. The electrical activity of TDs vanishes after thermal treatments above 500 °C [6]. The resistivity change of wafers due to such treatments can be used to assess the density of thermal donors (n_{TD}) [11].

The temperature dependent growth of nuclei to large scale precipitates is a well-studied topic due to its importance in microelectronics [6, 7, 12, 13]. Thereby precipitates can grow or dissolve depending on the absolute temperature, more precisely the critical radius r_c, which is increasing with temperature. Precipitates with a smaller radius than r_c dissolve and those with a higher radius grow. That results in a temperature dependent density and size distribution of precipitates. Furthermore, the growth is limited by the diffusion of interstitial oxygen (O_i) towards the precipitates [6, 7]. Small precipitates are assumed to have minor influence on τ_B until they reach a certain size, which causes mechanical stress in the surrounding silicon lattice. Thereby, the recombination activity scales with the surface area of strained precipitates [6, 14].

3 APPROACH

Symmetric carrier lifetime samples from large-area boron doped p-type Cz-Si as well as phosphorus doped n-type Cz-Si wafers from two different ingots, containing either a high or a low n_{TD} (pCz-highTD; pCz-lowTD; nCz-highTD and nCz-lowTD), are investigated in this experiment.

The process flow for the fabrication of symmetric carrier lifetime samples is shown in Figure 1. After saw damage etching, a first sheet resistance (R_{sh}) measurement of all wafers is done by means of eddy-current and a capacitive wafer thickness measurement to calculate the as-grown specific base resistivity $\rho_{B,1}$, which could be affected by the presence of TDs. After cleaning in hydrofluoric acid (HF), a variation of tube furnace diffusion processes using phosphorus

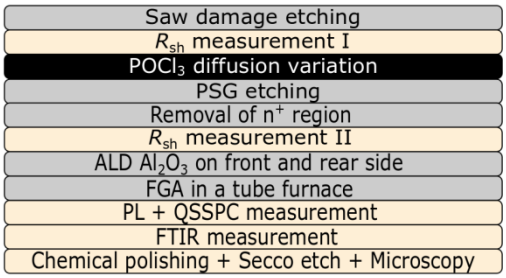

Figure 1: Process flow for the manufacturing of symmetric carrier lifetime samples fabricated from four different Cz-Si materials to investigate the influence of drive-in parameters of the $POCl_3$ diffusion on oxygen precipitation.

oxychloride ($POCl_3$) is performed as described below, whereby three wafers of each material are processed in each variation. All wafers undergo phosphor silicate glass (PSG) etching and an alkaline wet chemical etch to remove the diffused region. Afterwards, the second R_{sh} measurement and a capacitive wafer thickness measurement is performed to calculate $\rho_{B,2}$ after annihilation of TDs during the diffusion process. The two measurements $\rho_{B,1}$ and $\rho_{B,2}$ yield the thermal donor density n_{TD} [11]. This method takes the influence of the stronger carrier scattering through TDs and potential charge carrier compensation on charge mobility into account [15]. For carrier lifetime and photoluminescence (PL) measurements the wafers are passivated with an Al_2O_3 layer of 20 nm thickness, deposited via atomic layer deposition (ALD) on both sides of the wafers. A forming gas anneal (FGA) in a tube furnace activates the surface passivation. To keep the boron oxygen defects in the deactivated state [2], the samples are stored in the dark until the following measurements. PL imaging is used to study the lifetime distribution. Quasi steady state photoconductance decay (QSSPC) lifetime measurements are performed on five positions per wafer, to determine the average bulk lifetime τ_B, neglecting surface recombination. The bulk lifetimes are evaluated at a fixed excess carrier concentration of 10^{15} cm^{-3}. Finally, selected samples are analyzed using Fourier-transform infrared spectroscopy (FTIR) to determine the interstitial oxygen concentration n_{Oi}. These samples subsequently undergo a chemical polishing followed by a Secco etch for a duration of 70 s (~1,5 µm silicon per wafer side removed) to reveal etch pits related to oxygen precipitates [3]. The density of those etch pits is evaluated using a microscopy based method, giving the number of etch pits per unit area (EP_A).

Four different $POCl_3$ diffusion processes (P1-P4) are compared. They are performed in an industrial tube furnace with variations of the drive-in temperature $T_{drive\text{-}in}$ and drive-in duration $t_{drive\text{-}in}$, based on an industry relevant process (P1) [16], to analyze the effect on

Table I: Overview of the selected drive-in parameters for each of the five diffusion process variations.

Process	$T_{drive\text{-}in}$ / °C	$t_{drive\text{-}in}$ / min
P0	-	-
P1	860	12
P2	860	120
P3	1050	12
P4	1050	120

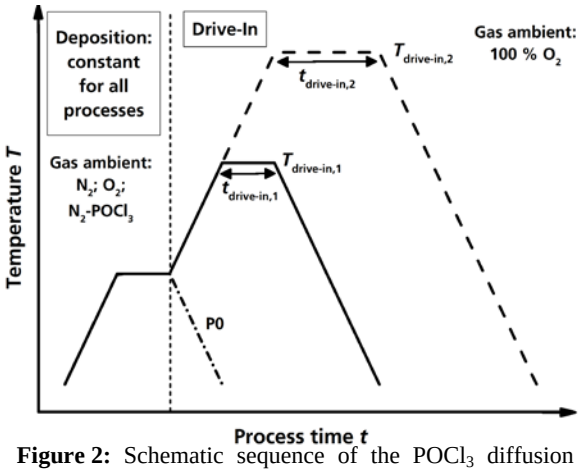

Figure 2: Schematic sequence of the $POCl_3$ diffusion processes performed in this work.

oxygen precipitation. Additionally, a reference group, with a tube furnace process P0 is considered, that only includes the growth sequence of the PSG layer, in the following denoted as deposition, while the drive-in step is skipped. Figure 2 depicts a schematic sequence of the $POCl_3$ diffusion processes and Table I summarizes the selected drive-in parameters. The first temperature plateau represents the PSG deposition sequence, which is similar for all performed processes. After this plateau the temperature ramps up reaching the drive-in plateau, while for process P0 the temperature ramps down reaching the unloading temperature. As depicted, the temperature $T_{drive\text{-}in}$ of the drive-in plateau is varied (860 °C or 1050 °C) as well as its duration $t_{drive\text{-}in}$ (12 min or 120 min). After that plateau the temperature is ramped down to the unloading temperature. The gas ambient introduced after the deposition phase consists of 100 % O_2 from ramp-up after deposition until reaching the unloading temperature. Before unloading, the furnace gets flushed with pure nitrogen at constant temperature.

4 RESULTS AND DISCUSSION

4.1 Thermal donor density n_{TD}

In Table II the average $\rho_{B,1}$ and $\rho_{B,2}$ values of all investigated materials, as well as the calculated n_{TD} are shown. As expected the highTD-materials show an increased n_{TD} compared to the lowTD-materials. Negligible n_{TD} are found for pCz-lowTD in accordance with expectations: since this material is produced by the magnetic Czochralski (mCz) technology [17] it contains less oxygen. A sufficient n_{Oi} is required for TD growth [6].

Table II: Average specific base resistivity in the as-grown state ($\rho_{B,1}$) and after thermal diffusion ($\rho_{B,2}$) of the different materials used in this experiment, as well as n_{TD} calculated according Ref [11].

Material	Type	$\rho_{B,1}$ / Ωcm	$\rho_{B,2}$ / Ωcm	n_{TD} / 10^{14} cm^{-3}
pCz-highTD	p-type Cz-Si	3.1	2.0	11.1
pCz-lowTD	p-type mCz-Si	0.6	0.6	0.0
nCz-highTD	n-type Cz-Si	2.0	10.5	10.1
nCz-lowTD	n-type Cz-Si	5.4	5.9	0.4

4.2 Bulk lifetime τ_B

Figure 3 shows the PL images of one sample per Cz-Si material for all diffusion processes. The images are scaled individually for better visualization of the observed patterns. While pCz-lowTD and nCz-lowTD do not exhibit any circular defect patterns after all processes, pCz-highTD and nCz-highTD show a dark circular area after the processes P2, P3 and P4 while only the corners of the samples show a significant PL signal.

For nCz-highTD, circular defect patterns can already be seen after process P1, which indicates a notable defect at $T_{drive\text{-}in}$ = 860 °C even for $t_{drive\text{-}in}$ = 12 min. With increasing $t_{drive\text{-}in}$ (compare P1 and P2) and with increasing $T_{drive\text{-}in}$ (compare P1 and P3) the PL signal in both highTD-materials gets drastically reduced. For pCz-highTD a further reduction can be seen with increasing $t_{drive\text{-}in}$ at $T_{drive\text{-}in}$ = 1050 °C (compare P3 and P4), while for nCz-highTD no further reduction is visible. The scratches, dark areas and the reduction in PL signal towards the edges, visible at all images of the lowTD-materials as well as after processes P0 and P1 of the highTD-materials, originate from wafer handling, passivation inhomogeneities and PL vignetting, respectively and are not attributed to bulk defects.

The PL results correlate to the measured bulk lifetime τ_B, whereat in the following only τ_B of the highTD-materials is presented. After the PSG deposition process (P0), both highTD materials show the highest bulk lifetime values with τ_B = 0.34 ms for pCz-highTD and τ_B = 4.85 ms for nCz-highTD. In Figure 4 τ_B is shown for the processes P1 to P4 of both highTD-materials, plotted against $T_{drive\text{-}in}$. For both materials, a strong dependence of $T_{drive\text{-}in}$ and $t_{drive\text{-}in}$ can be seen. With increasing $T_{drive\text{-}in}$ as well as increasing $t_{drive\text{-}in}$ the τ_B gets drastically reduced.

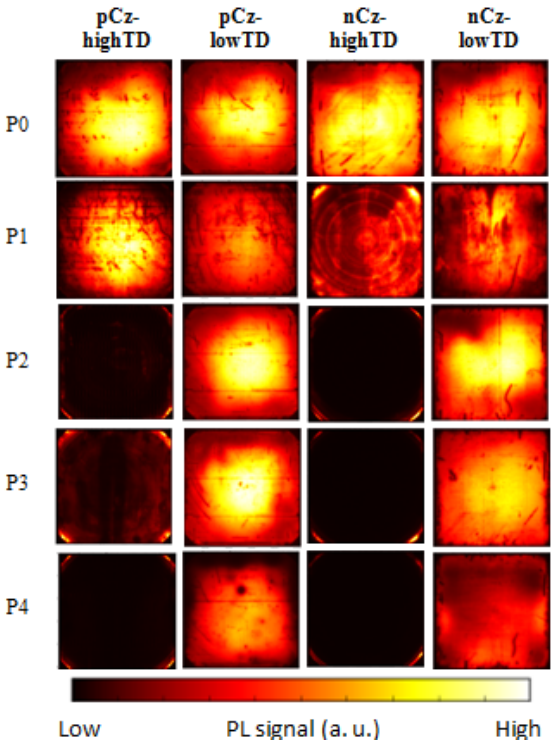

Figure 3: Individually scaled PL images of one sample of all processes for every investigated material. The measurement is performed at 1 sun illumination after removal of the n^+ region and passivation.

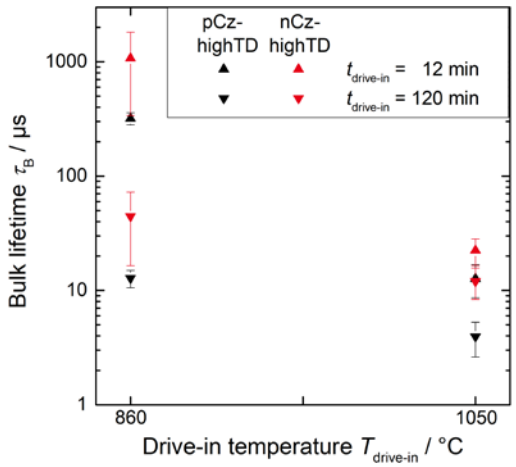

Figure 4: Average bulk lifetime τ_B and standard deviation for materials pCz-highTD and nCz-highTD for the processes P1-P4 (see Table I), plotted against $T_{drive\text{-}in}$. The lifetimes are evaluated at a fixed excess carrier concentration of 10^{15} cm^{-3} and after dark annealing (deactivated state of boron oxygen defects in p-type material).

The fact that only the highTD-materials exhibit the circular defect pattern in PL measurements confirms the correlation between the n_{TD} and the susceptibility of the material to form oxygen precipitates. The dependence of τ_B on $T_{drive\text{-}in}$ and $t_{drive\text{-}in}$ can be attributed to the diffusion limited growth of precipitates, which is discussed in section 4.4.

4.3 Interstitial oxygen concentration n_{Oi}

According to literature the growth of oxygen precipitates and thus the incorporation of interstitial oxygen O_i into the precipitates is diffusion limited [6, 7]. Samples from both processes with $t_{drive\text{-}in}$ = 120 min (P2 and P4) as well as from process P0 of every investigated material are measured by FTIR. Figure 5 depicts the measured n_{Oi}, with materials pCz-lowTD and

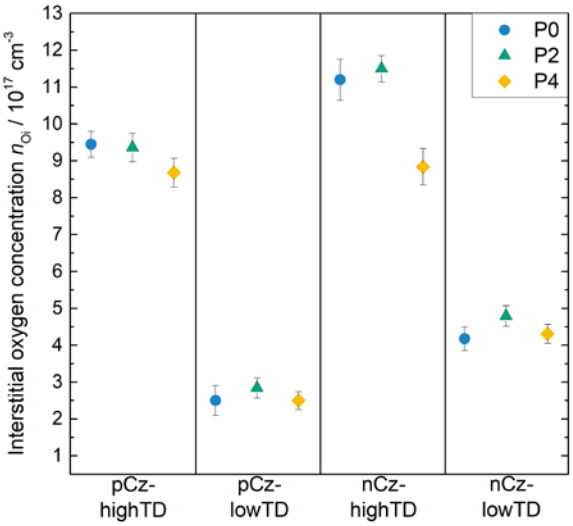

Figure 5: Interstitial oxygen concentration n_{Oi} measured by FTIR in samples for processes P0, P2 and P4 of every investigated material. The measurement is performed with one sample per group after removal of the n^+ region and passivation, whereby the average value of a 5 cm x 5 cm field is depicted.

nCz-lowTD exhibiting rather low concentrations of $2.5 \cdot 10^{17}$ cm^{-3} < n_{Oi} < $2.8 \cdot 10^{17}$ cm^{-3} and $4.2 \cdot 10^{17}$ cm^{-3} < n_{Oi} < $4.8 \cdot 10^{17}$ cm^{-3}, respectively. The highTD-wafers show factor 2 to 4 higher n_{Oi} compared to the lowTD-wafers for all three processes. This agrees well with the observed n_{TD} in the materials, as discussed above. While pCz-lowTD and nCz-lowTD show no significant change in n_{Oi} for the different processes, n_{Oi} decreases notably from process P0 to P4 for both pCz-highTD and nCz-highTD. Thereby the n_{Oi} decreases from $n_{Oi} = 9.5 \cdot 10^{17}$ cm^{-3} to $n_{Oi} = 8.7 \cdot 10^{17}$ cm^{-3} for pCz-highTD and from $n_{Oi} = 11.2 \cdot 10^{17}$ cm^{-3} to $n_{Oi} = 8.8 \cdot 10^{17}$ cm^{-3} for nCz-highTD.

The n_{Oi} in the lowTD-materials is not changing significantly as low interstitial oxygen concentrations reduce the driving force for oxygen precipitation. The decrease of n_{Oi} in the highTD-materials can be explained by the growth of precipitates, which indicates that the circular defect pattern in Figure 3 and the resulting decrease of τ_B (see Figure 4) is attributed to oxygen precipitation.

4.4 Oxygen diffusion length L_{Oi}

As shown above, both parameters, $T_{drive\text{-}in}$ and $t_{drive\text{-}in}$ have a strong impact on the oxygen precipitation. Therefore, we cannot easily predict the oxygen precipitation potential for a given arbitrary temperature-time profile. The growth of oxygen precipitates is limited by the diffusion of interstitial oxygen to the precipitation site [6, 7]. Therefore, we suggest to assess the process specific oxygen diffusion length L_{Oi} as a measure for precipitation risk.

Based on the analysis of Borghesi [6], we assume concentration gradient and temperature dependent diffusion with a diffusion constant of $D_0 = 0.13$ cm^2/s and an activation energy of $E_D = 2.53$ eV.

For calculating L_{Oi}, the equation for the diffusion length

$$L = \sqrt{D \cdot t} \qquad \text{Eq. 1}$$

with

$$D = D_0 \cdot e^{\left(-\frac{E_D}{kT}\right)} \qquad \text{Eq. 2}$$

is used. Thereby t is the diffusion time, D the diffusion coefficient, k the Boltzmann constant and T the diffusion temperature. Derived from Eq. 1, L_{Oi} is integrated over the temperature profile of the diffusion process, using

$$L_{Oi} = \int_{t_0}^{t_1} \frac{\sqrt{D\left(T(t)\right)}}{2\sqrt{t}} dt \qquad \text{Eq. 3}$$

with t_0 and t_1 being the start and end process time, respectively and $T(t)$ the temperature-time profile.

The change in bulk carrier recombination R_B is calculated for every diffusion process (P1-P4) using

$$R_B = \frac{1}{\tau_B} - \frac{1}{\tau_{B,P0}} \qquad \text{Eq. 4}$$

with τ_B being the average bulk lifetime of each diffusion variation (P1 to P4) and $\tau_{B,P0}$ the average bulk lifetime of the process group P0. The lifetimes are evaluated at a fixed excess carrier concentration of 10^{15} cm^{-3} and thereby recombination changes due to the process are evaluated, while influences such as surface recombination are corrected for. R_B therefore quantifies the increase in bulk recombination induced by the drive-in sequence.

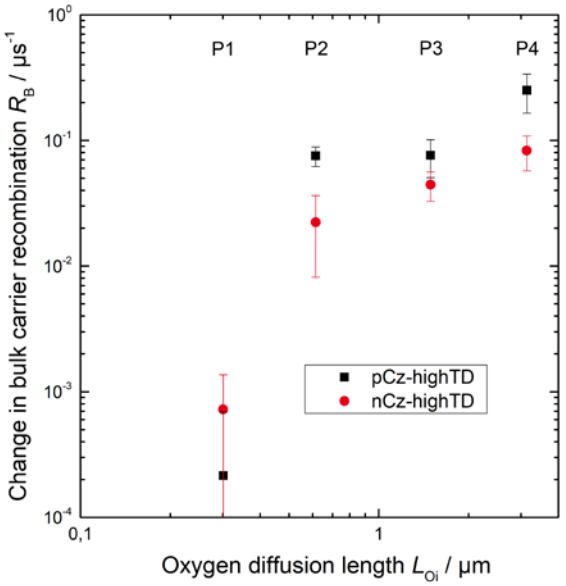

Figure 6: Change in bulk carrier recombination R_B and standard deviation derived by Gaussian error propagation of the diffusion processes P1 to P4, plotted over the corresponding oxygen diffusion length L_{Oi} for materials pCz-highTD and nCz-highTD.

In Fig. 6 the R_B of every diffusion process (P1-P4) is plotted over the corresponding L_{Oi} for materials pCz-highTD and nCz-highTD. Both materials show the same behavior. R_B increases with L_{Oi}. A steep increase from $L_{Oi} = 0.3$ µm (P1) to $L_{Oi} = 0.6$ µm (P2) can be seen for both materials, where R_B increases from $R_B = 2 \cdot 10^{-4}$ µs^{-1} to $R_B = 7.5 \cdot 10^{-2}$ µs^{-1} for pCz-highTD and from $R_B = 7 \cdot 10^{-4}$ µs^{-1} to $R_B = 2.2 \cdot 10^{-2}$ µs^{-1} for nCz-highTD. At $L_{Oi} > 0.6$ µm the slope gets reduced and increases to $R_B = 2.5 \cdot 10^{-1}$ µs^{-1} for pCz-highTD and $R_B = 8.3 \cdot 10^{-2}$ µs^{-1} for nCz-highTD at $L_{Oi} = 3.1$ µm.

The increase in R_B with L_{Oi} can be attributed to the diffusion limited growth of precipitates. According to the literature, the recombination activity increases with precipitate surface area after their radius excees a critical size leading to mechanical stress in the surrounding silicon lattice [6, 14].

4.5 Number of etch pits per unit area EP_A

For all processes (P0 to P4) of pCz-hightTD as well as for processes P0 and P4 of pCz-lowTD a Secco etch of one sample is performed. Due to the Secco etch lattice defects in crystalline silicon are etched, leading to etch pits.

In Figure 7 a microscopy photograph of one sample of the processes P0 and P4 for material pCz-highTD after Secco etch is depicted. Thereby the surface structure, visible in both photographs, results from chemical polishing. After process P0 no etch-pits can be seen, while after process P4 a significant amount of etch-pits is visible. To quantify the etch-pits, a 1 mm wide stripe

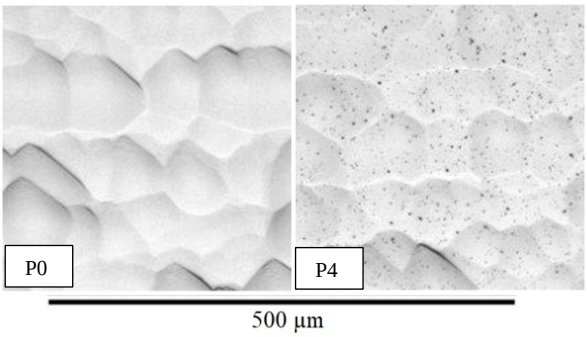

Figure 7: Microscopy photograph of one sample of process P0 and P8 for material pCz-highTD after Secco etch. The photograph is taken in the center of the samples.

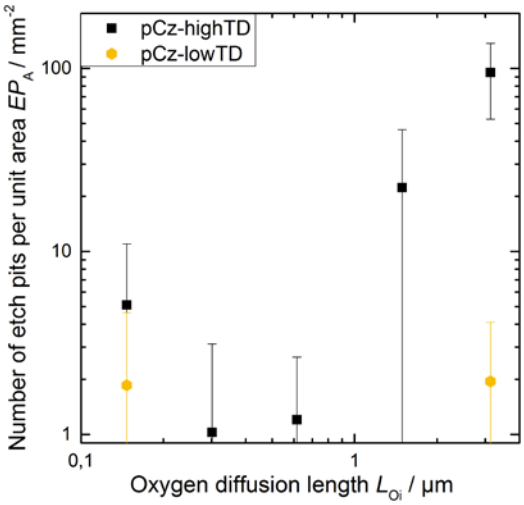

Figure 8: Number of etch-pits per unit area EP_A of one sample of all processes of material pCz-highTD and of processes P0 and P4 of material pCz-lowTD, plotted against the corresponding L_{Oi}.

from the center of each sample was scanned and the number of etch pits evaluated using an image tool. Because of the circular defect pattern (see Figure 3), this measurement is leading to a representative value for the whole sample. To reduce false detection, only etch-pits with an area between 6 µm^2 and 30 µm^2 are counted. In Figure 8 the EP_A of one sample of all processes of material pCz-highTD and of processes P0 and P4 of material pCz-lowTD is plotted over the corresponding L_{Oi}. For material pCz-lowTD a very low $EP_A \approx 2$ mm^{-2} is measured, while no significant change can be seen with increasing L_{Oi}. For material pCz-highTD EP_A drastically increases with L_{Oi} from $EP_A < 5$ mm^{-2} for $L_{Oi} < 0.6$ µm to $EP_A \approx 100$ mm^{-2} for $L_{Oi} = 3.1$ µm.

The Secco etch can only indicate strained oxygen precipitates. Due to the growth of precipitates more etch-pits are visible after the processes with higher L_{Oi} in material pCz-highTD. This correlates well to the appearance of the circular defect pattern in PL measurements (see Figure 3), the interstitial oxygen consumption (see Figure 5) and the increase in R_B (see Figure 6). No significant amount of etch pits could be detected for process P2 with $L_{Oi} = 0.6$ µm , while R_B is already at a high value of $R_B = 7.5 \cdot 10^{-2}$ µs^{-1}. This suggests that oxygen precipitates are already affecting τ_B before reaching a size that can be detected in our setup after Secco etch. For material pCz-lowTD no significant change in EP_A could be detected, supporting the expectation that no precipitates are growing.

5 SUMMARY

In this work we investigate the impact of the diffusion process drive-in temperature and duration on the formation of recombination active oxygen precipitates in different Cz-Si wafers. As known from literature, increasing temperature and duration show significant impact on the oxygen precipitation. Especially vacancy rich Cz-Si wafers with a high grown-in density of thermal donors tend to form ring defect structures when subjected to a high thermal budget.

We apply the process specific oxygen diffusion length L_{Oi} as an indicator whether the growth of oxygen precipitates is to be expected on prone material for a given temperature-time-profile of the $POCl_3$ diffusion process. Our data shows that this quantity correlates with both, the process induced bulk recombination and the etch pit density, which shows that L_{Oi} is a plausible parameter to predict the potential of a thermal process to grow existing oxygen precipitates. Please note that this parameter does not consider the temperature dependent dissolution of precipitates and the nucleation of new precipitates. However, for process temperatures above 750°C nucleation is expected to be negligible.

Furthermore, we observed similar oxygen precipitation in the tested p-type and n-type Cz-Si. To avoid cell efficiency losses in p-type as well as n-type Cz-Si solar cells due to oxygen precipitation, the L_{Oi} of the diffusion process should be small. We propose a threshold of $L_{Oi} < 0.3$ µm to avoid unintentional precipitation. That will support increased production yield for Cz-Si based solar cells, for instance PERC cells.

ACKNOWLEDGEMENTS

The authors thank all colleagues at the Fraunhofer ISE, especially S. Schmidt, D. Herrmann and F. Schindler.

This work was funded by the German Federal Ministry for Economic Affairs and Energy BMWi in projects “POLDI” (contract number 0324079D) and “GENESIS” (contract numbers 0324274C and 0324274E).

REFERENCES

[1] ITRPV consortium, “International Technology Roadman for Photovoltaic (ITRPV): Results 2018, 10th edition,” 10th Edition, 2019.

[2] K. Krauss, “Multicrystalline Silicon Solar Cell Concepts and Light-Induced Degradation,” Dissertation, Fraunhofer Institute for Solar Energy Systems ISE, University of Freiburg, Freiburg, 2017.

[3] L. Chen *et al.*, “Effect of oxygen precipitation on the performance of Czochralski silicon solar cells,” *Solar Energy Materials and Solar Cells*, vol. 95, no. 11, pp. 3148–3151, 2011.

[4] T. Niewelt *et al.*, “Light-induced activation and deactivation of bulk defects in boron-doped float-zone silicon,” *Journal of Applied Physics*, vol. 121, no. 18, p. 185702, 2017.

[5] A. Bentzen, “Phosphorus diffusion and gettering in silicon solar cells,” Dissertation, Department of Physics, Oslo, University of, Oslo, 2006.
[6] A. Borghesi, B. Pivac, A. Sassella, and A. Stella, “Oxygen precipitation in silicon,” *Journal of Applied Physics*, vol. 77, no. 9, pp. 4169–4244, 1995.
[7] R. C. Newman, “Oxygen diffusion and precipitation in Czochralski silicon,” *Journal of Physics: Condensed Matter*, vol. 12, no. 25, R335-65, 2000.
[8] J. Haunschild, J. Broisch, I. Reis, and S. Rein, “Cz-Si wafers in solar cell production: Efficiency-limiting defects and material quality control,” *Photovoltaics International*, no. 15, pp. 40–46, 2012.
[9] J. Schön *et al.*, “Identification of lifetime limiting defects by temperature- and injection-dependent photoluminescence imaging,” *Journal of Applied Physics*, vol. 120, no. 10, p. 105703, 2016.
[10] F. Korsós *et al.*, “Efficiency limiting crystal defects in monocrystalline silicon and their characterization in production,” *Solar Energy Materials and Solar Cells*, vol. 186, pp. 217–226, 2018.
[11] T. Niewelt *et al.*, “Interstitial oxygen imaging from thermal donor growth—A fast photoluminescence based method,” *Sol. Energy Mater. Sol. Cells*, vol. 131, pp. 117–123, 2014.
[12] R. J. Falster, M. Cornara, D. Gambaro, M. Olmo, and M. Pagani, “Effect of High Temperature Pre-Anneal on Oxygen Precipitates Nucleation Kinetics in Si,” *SSP*, vol. 57-58, pp. 123–128, 1997.
[13] V. LaSalvia *et al.*, “Tabula Rasa for n -Cz silicon-based photovoltaics,” *Prog Photovolt Res Appl*, vol. 70, no. 12, p. 1572, 2018.
[14] J. D. Murphy *et al.*, “The effect of oxide precipitates on minority carrier lifetime in n -type silicon,” *Journal of Applied Physics*, vol. 118, no. 21, p. 215706, 2015.
[15] F. Schindler *et al.*, “Towards a unified low-field model for carrier mobilities in crystalline silicon,” *Sol. Energy Mater. Sol. Cells*, vol. 131, pp. 92–99, 2014.
[16] S. Werner, S. Mourad, W. Hasan, and A. Wolf, “Structure and composition of phosphosilicate glass systems formed by POCl 3 diffusion,” *Energy Procedia*, vol. 124, pp. 455–463, 2017.
[17] F. Mosel *et al.*, “Growth of high quality silicon mono ingots by the application of a magnetic cusp field in cz-puller,” in *27th EU PVSEC*, Frankfurt, 2012, pp. 933–938.